SEISMIC RESPONSE AND DESIGN OF ARCHED STRUCTURES

George C. Tsiatas[1] and Michalis Fragiadakis[2]

[1]School of Civil Engineering
National Technical University of Athens
Athens, GR-15773, Greece
e-mail: gtsiatas@gmail.com ; web page: http://users.ntua.gr/gtsiatas

[2]School of Civil Engineering
National Technical University of Athens
Athens, GR-15773, Greece
e-mail: mfrag@mail.ntua.gr ; web page: http://users.ntua.gr/mfrag

Keywords: Arched structures, Non-uniform arches, Response history analysis, Analog Equation Method, Seismic analysis.

Abstract. *The aim of this paper is to investigate the dynamic response of arched structures and to revisit their seismic design. Arches are often used in real world applications (e.g. bridges, roofs) to span large areas by resolving vertical forces into compressive stresses and confining tensile stresses. The full understanding of the dynamic response of such structures poses a challenging technical and computational problem, especially when seismic loading is considered. For example, the assumption of axial inextensibility, although leads to a simplified sixth order differential equation overestimates the vibration frequencies, especially those of shallow arches. In our study, arched structures are modeled with a generic approach that includes both axial (tangential) and transverse (normal) deformation, variable mass and stiffness properties, as well as elastic support or restraint. The resulting dynamic governing equations of the arch are formulated in terms of the displacements, and solved using an efficient integral equation method. Several arches are analyzed in order to investigate their dynamic properties and to efficiently assess their capacity using response history analysis.*

1 INTRODUCTION

Arched structures of constant or variable geometric properties are quite often encountered in real world applications such as bridges, roofs, etc. Mainly, arches exhibit advantageous behavior over straight beams due to their curved centerline which increases the overall stiffness of the structure. They are used to span large areas by resolving vertical forces into compressive stresses and confining tensile stresses. The full understanding of the dynamic response of such structures poses a challenging technical and computational problem, especially when seismic loading is considered. To mitigate this complex problem, several investigators adopted the inextensionality condition which neglects the axial deformation of the arch. Among them Laura and Verniere de Irassar [1], Gutierrez et al. [2], Tong et al. [3], Shin et al. [4] studied the free vibration problem of inextensional circular arches with variable cross-section by solving one reduced equation of motion instead of two coupled ones. The influence of axial deformation was investigated by Chidamparam and Leissa [5] which concluded that may have a profound effect especially in the study of shallow arches in which the vibration frequencies are overestimated.

On the other hand, the work published on the seismic response of arched structures is rather limited. Dusseau et al. [6] studied the dynamic responses of three deck-type steel arch bridges by applying artificial ground motions in three directions to their finite-element models of each bridge. It was found that responses to uniform lateral motion were generally the largest, while the responses to vertical motion were generally lower than those due to lateral or longitudinal motion. Hao [7] analysed the in-plane stochastic responses of incompressible uniform circular arches to spatially correlated horizontal multiple excitations and his results indicate that the responses may be underestimated or overestimated by neglecting the ground motion spatial variations. Hao [8] extended his previous work to analyse the responses of the incompressible circular arches to correlated simultaneous horizontal and vertical multiple excitations. He found that vertical ground motion component might have significant effect on the arch responses. Usami et al. [9, 10] studied the inelastic behavior of steel arch bridges subjected to strong ground motions from major earthquakes. They drew the conclusion that, the transverse direction of arch bridges is more dangerous than the longitudinal direction under earthquake excitations.

The rationale of this work is to perform a comprehensive study over the complicated seismic behavior of arched beam structures due to their coupled displacement field. The present study reveals the dynamic

performance of such structures using a new curved beam model which is based on a generic approach and is alleviated of the known inextensionality condition. Within this context, the proposed model includes both axial (tangential) and transverse (normal) deformation, variable mass and stiffness properties, as well as elastic support or restraint. The resulting dynamic governing equations of the arch are formulated in terms of the displacements, and solved using an efficient integral equation method. Several arches are analyzed in order to investigate their dynamic properties and to efficiently assess their capacity using response history analysis.

2 PROBLEM FORMULATION

In this section, the fundamental equations governing the dynamic response of non-uniform arches together with their respective boundary conditions and initial conditions are derived in terms of the displacements. The employed generic model includes both axial (tangential) and transverse (normal) deformation, variable mass and stiffness properties, as well as elastic support or restraint.

2.1 Equilibrium equations

Let us consider a plane curved beam the cross-sections of which are orthogonal to a plane curve (centroid axis) that belongs to the xz plane. A curvilinear abscissa s spans the beam's centroid axis which is bent in its plane under the combined action of the distributed loads $p_t = p_t(s)$ and $p_n = p_n(s)$ acting in the tangential and normal direction, respectively (see Fig. 1). The beam may have a non-uniform cross-section, that is the axial $EA(s)$ and bending stiffness $EI(s)$ vary due to variable cross-sectional properties, $A = A(s)$, $I = I(s)$, and/or nonhomogeneous linearly elastic material $E = E(s)$.

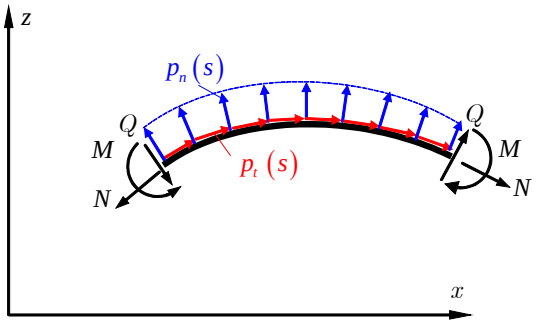

Figure 1. Positive forces and moments acting on a curved element.

The governing equations of the curved beam are derived by considering the equilibrium of an elementary section of length ds, in projections onto the tangential t and the normal n directions and in moments with respect to one of the beam's ends. In this way, we arrive at the following equations [11]

$$-m\ddot{u} - c\dot{u} + N_{,s} + \frac{Q}{R} = -p_t \tag{1}$$

$$-m\ddot{w} - c\dot{w} + Q_{,s} - \frac{N}{R} = -p_n \tag{2}$$

$$M_{,s} = Q \tag{3}$$

where $m = m(s) = \rho A(s)$ is the mass density per unit length, c is the coefficient of viscous damping, R is the radius of the arch; $u(s)$ and $w = w(s)$ are the tangential and normal displacements, respectively.

Further, the axial force and the bending moment are integral stress resultants which are calculated by the following formulae

$$N = \int_A \sigma_s dA \tag{4}$$

$$M = \int_A \sigma_s z dA \tag{5}$$

where

$$\sigma_s = E\varepsilon_s \tag{6}$$

is the normal stress and ε_s is the normal strain along the z-coordinate. According to the Vlasov's engineering theory the linear strain distribution is given by

$$\varepsilon_s(s,z) = \varepsilon_0 + \chi z - \frac{\chi}{R} z^2 \tag{7}$$

where

$$\varepsilon_0(s,0) = u_{,s} + \frac{w}{R} \tag{8}$$

is the longitudinal and

$$\chi = -w_{,ss} - \frac{w}{R^2} \tag{9}$$

is the flexural component of strain.

By substituting eqs (6)–(9) into eqs (4) and (5), and using eqn (3), the stress resultant–displacement relationships are obtained as

$$N = EA\left(u_{,s} + \frac{w}{R}\right) + \frac{EI}{R}\left(w_{,ss} + \frac{w}{R^2}\right) \tag{10}$$

$$M = -EI\left(w_{,ss} + \frac{w}{R^2}\right) \tag{11}$$

$$Q = -EI\left(w_{,sss} + \frac{w_{,s}}{R^2}\right) - (EI)_{,s}\left(w_{,ss} + \frac{w}{R^2}\right) \tag{12}$$

Finally, by substituting eqs (10)-(12) into eqs (1) and (2), and using eqn (3) to eliminate Q, we obtain the equilibrium equations in terms of displacements as follows

$$-m\ddot{u} - c\dot{u} + \left[EA\left(u_{,s} + \frac{w}{R}\right)\right]_{,s} = -p_t \tag{13}$$

$$-m\ddot{w} - c\dot{w} - \left[EI\left(w_{,ss} + \frac{w}{R^2}\right)\right]_{,ss} - \frac{1}{R}\left[EA\left(u_{,s} + \frac{w}{R}\right) + \frac{EI}{R}\left(w_{,ss} + \frac{w}{R^2}\right)\right] = -p_n \tag{14}$$

2.2 Boundary conditions

The boundary conditions of the problem, that can include elastic support or restraint, are of the form

$$a_1 u(0,t) + a_2 N(0,t) = 0, \quad \bar{a}_1 u(l,t) + \bar{a}_2 N(l,t) = 0 \tag{15), (16}$$

$$\beta_1 w(0,t) + \beta_2 Q(0,t) = 0, \quad \bar{\beta}_1 w(l,t) + \bar{\beta}_2 Q(l,t) = 0 \tag{17), (18}$$

$$\gamma_1 \theta(0,t) + \gamma_2 M(0,t) = 0, \quad \bar{\gamma}_1 \theta(l,t) + \bar{\gamma}_2 M(l,t) = 0 \tag{19), (20}$$

where $a_k, \bar{a}_k, \beta_k, \bar{\beta}_k, \gamma_k, \bar{\gamma}_k$ $(k = 1,2)$ are given constants and $\theta = -w_{,s} + u/R$ is the slope of the cross-section [11]. It is apparent that all types of the conventional boundary conditions (clamped, simply supported etc.) can be derived from eqs (15)-(20) by specifying appropriately these constants.

2.3 Initial conditions

The pertinent initial conditions of the problem are

$$u(s,0) = \tilde{u}(s), \quad \dot{u}(s,0) = \dot{\tilde{u}}(s) \tag{21), (22}$$

$$\tilde{w}(s,0) = \tilde{w}(s), \quad \dot{\tilde{w}}(s,0) = \dot{\tilde{w}}(s) \tag{23), (24}$$

where $\tilde{u}(s)$, $\dot{\tilde{u}}(s)$, $\tilde{w}(s)$ and $\dot{\tilde{w}}(s)$ are prescribed functions.

3 THE AEM SOLUTION FOR THE DYNAMIC ANALYSIS OF ARCHES

The initial boundary value problem described by eqs (13) - (24) is solved using the AEM [12, 13], a robust numerical method based on an integral equation technique. The analog equations for the problem at hand are

$$u_{,ss} = b_1(s,t) \tag{25}$$

$$w_{,ssss} = b_2(s,t) \tag{26}$$

Eqs (25) and (26) describe the axial and bending linear response of a beam with constant unit axial and flexural stiffness subjected to the unknown fictitious axial b_1 and transverse b_2 loads, respectively, depending also in time. The solution of eqs (25) and (26) at a point $s \in (0,l)$ is obtained in integral form as

$$u(s,t) = c_1 s + c_2 + \int_0^l G_1(s,\xi) b_1(\xi,t)\, d\xi \tag{27}$$

$$w(s,t) = c_3 s^3 + c_4 s^2 + c_5 s + c_6 + \int_0^l G_2(s,\xi) b_2(\xi,t)\, d\xi \tag{28}$$

where c_i $(i = 1,2,...6)$ are arbitrary time-dependent integration constants to be determined from the boundary conditions and $G_1 = \frac{1}{2}|s-\xi|$, $G_2 = \frac{1}{12}|s-\xi|(s-\xi)^2$ are the fundamental solutions (free space Green's functions) of Eqs. (25) and (26), respectively.

The derivatives of u and w are obtained by direct differentiation of Eqs. (27) and (28). Thus, we have

$$u_{,s}(s,t) = c_1 + \int_0^l G_{1,s}(s,\xi) b_1(\xi,t)\, d\xi, \qquad u_{,ss}(s,t) = b_1(s,t) \tag{29), (30}$$

$$w_{,s}(s,t) = 3c_3 s^2 + 2c_4 s + c_5 + \int_0^l G_{2,s}(s,\xi) b_2(\xi,t)\, d\xi \tag{31}$$

$$w_{,ss}(s,t) = 6c_3 s + 2c_4 + \int_0^l G_{2,ss}(s,\xi) b_2(\xi,t)\, d\xi \tag{32}$$

$$w_{,sss}(s,t) = 6c_3 + \int_0^l G_{2,sss}(s,\xi) b_2(\xi,t)\, d\xi, \qquad w_{,ssss}(s,t) = b_2(s,t) \tag{33), (34}$$

Substituting eqs (27) - (34) into eqs (13) and (14) yields the equations, from which the fictitious sources b_1 and b_2 can be determined. This can be implemented only numerically as follows.

The interval $(0,l)$ is divided into N equal elements (see Fig. 2) on which b_1 and b_2 are assumed constant. After discretization of Eqs. (27) and (28) we obtain

$$u(s,t) = \mathbf{H}_1(s)\mathbf{c}_1 + \mathbf{G}_1(s)\mathbf{b}_1, \quad w(s,t) = \mathbf{H}_2(s)\mathbf{c}_2 + \mathbf{G}_2(s)\mathbf{b}_2 \tag{35), (36}$$

where $\mathbf{G}_1(s)$ and $\mathbf{G}_2(s)$ are $1\times N$ known matrices originating from the integration of the kernels $G_1(s,\xi)$ and $G_2(s,\xi)$ on the elements, respectively; $\mathbf{H}_1(s) = [s \quad 1]$ and $\mathbf{H}_2(s) = [s^3 \quad s^2 \quad s \quad 1]$; $\mathbf{c}_1 = \{c_1, c_2\}^T$; $\mathbf{c}_2 = \{c_3, c_4, c_5, c_6\}^T$; $\mathbf{b}_1$, $\mathbf{b}_2$ are the vectors containing the values of the fictitious loads at the nodal points, respectively. Similarly, we obtain for eqs (29) - (34)

$$u_{,s}(s,t) = \mathbf{H}_{1s}(s)\mathbf{c}_1 + \mathbf{G}_{1s}(s)\mathbf{b}_1, \quad u_{,ss}(s,t) = \mathbf{b}_1 \tag{37), (38}$$

$$w_{,s}(s,t) = \mathbf{H}_{2s}(s)\mathbf{c}_2 + \mathbf{G}_{2s}(s)\mathbf{b}_2, \quad w_{,ss}(s,t) = \mathbf{H}_{2ss}(s)\mathbf{c}_2 + \mathbf{G}_{2ss}(s)\mathbf{b}_2 \tag{39), (40}$$

$$w_{,sss}(s,t) = \mathbf{H}_{2sss}(s)\mathbf{c}_2 + \mathbf{G}_{2sss}(s)\mathbf{b}_2, \quad w_{,ssss}(s,t) = \mathbf{b}_2 \tag{41), (42}$$

where $\mathbf{G}_{1s}(s)$, $\mathbf{G}_{2s}(s)$, $\mathbf{G}_{2ss}(s)$, $\mathbf{G}_{2sss}(s)$ are $1\times N$ known matrices, originating from the integration of the derivatives of the kernels $G_1(s,\xi)$, $G_2(s,\xi)$ on the elements; $\mathbf{H}_{1s}(s)$ is a 1×2 known matrix resulting from the differentiation of $\mathbf{H}_1(s)$, whereas $\mathbf{H}_{2s}(s)$, $\mathbf{H}_{2ss}(s)$, $\mathbf{H}_{2sss}(s)$ are 1×4 known matrices resulting from the differentiation of $\mathbf{H}_2(s)$.

First, eqs (35) - (42) are applied to the arch end nodal points $s = 0$ and $s = l$ and afterwards they are substituted to the coupled boundary conditions eqs (15) - (20) to express $\mathbf{c}_1$, $\mathbf{c}_2$ in terms of $\mathbf{b}_1$, $\mathbf{b}_2$. The latter equations are used to eliminate $\mathbf{c}_1$, $\mathbf{c}_2$ from eqs (35) - (42) which are eventually take the form

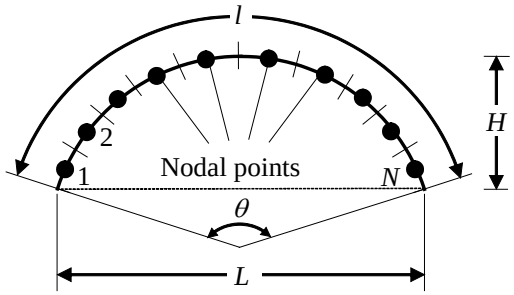

Figure 2. Arch geometry, descritization of the interval and distribution of the nodal points.

$$\mathbf{u} = \mathbf{T}_1\mathbf{b}_1, \quad \mathbf{w} = \mathbf{T}_2\mathbf{b}_2, \tag{43), (44}$$

$$\mathbf{u}_{,s} = \mathbf{T}_{1s}\mathbf{b}_1, \quad \mathbf{u}_{,ss} = \mathbf{b}_1, \quad \mathbf{w}_{,s} = \mathbf{T}_{2s}\mathbf{b}_2, \tag{45), (46), (47}$$

$$\mathbf{w}_{,ss} = \mathbf{T}_{2ss}\mathbf{b}_2, \quad \mathbf{w}_{,sss} = \mathbf{T}_{2sss}\mathbf{b}_2, \quad \mathbf{w}_{,ssss} = \mathbf{b}_2 \tag{48), (49), (50}$$

where $\mathbf{T}_1$, $\mathbf{T}_{1s}$, $\mathbf{T}_2$, $\mathbf{T}_{2s}$, $\mathbf{T}_{2ss}$, $\mathbf{T}_{2sss}$ are known $N \times N$ matrices.

Furthermore, the first and second derivatives of the displacements with respect to time can be obtained by direct differentiation of eqs (43) and (44). That is,

$$\dot{\mathbf{u}} = \mathbf{T}_1\dot{\mathbf{b}}_1, \quad \ddot{\mathbf{u}} = \mathbf{T}_1\ddot{\mathbf{b}}_1, \tag{51), (52}$$

$$\dot{\mathbf{w}} = \mathbf{T}_2\dot{\mathbf{b}}_2, \quad \ddot{\mathbf{w}} = \mathbf{T}_2\ddot{\mathbf{b}}_2 \tag{53), (54}$$

The final step of AEM is to apply eqs (13) and (14) to the N nodal points (see Fig. 2) and substitute the displacements and their derivatives on the basis of eqs (43) - (50). Thus, we obtain the semi-discretized equation of motion

$$\begin{bmatrix} \mathbf{m} & \mathbf{0} \\ \mathbf{0} & \mathbf{m} \end{bmatrix}\begin{bmatrix} \ddot{\mathbf{b}}_1 \\ \ddot{\mathbf{b}}_2 \end{bmatrix} + \begin{bmatrix} \mathbf{c}_1 & \mathbf{0} \\ \mathbf{0} & \mathbf{c}_2 \end{bmatrix}\begin{bmatrix} \dot{\mathbf{b}}_1 \\ \dot{\mathbf{b}}_2 \end{bmatrix} + \begin{bmatrix} \mathbf{k}_{11} & \mathbf{k}_{12} \\ \mathbf{k}_{21} & \mathbf{k}_{22} \end{bmatrix}\begin{bmatrix} \mathbf{b}_1 \\ \mathbf{b}_2 \end{bmatrix} = \begin{bmatrix} \mathbf{p}_t \\ \mathbf{p}_n \end{bmatrix} \tag{55}$$

where $\mathbf{m}$, $\mathbf{c}_1$, $\mathbf{c}_2$, $\mathbf{k}_{11}$, $\mathbf{k}_{12}$, $\mathbf{k}_{21}$, $\mathbf{k}_{22}$ are known $N \times N$ matrices, and $\mathbf{p}_t$, $\mathbf{p}_n$ are vectors containing the values of the dynamic external loading at the N nodal points. This formulation, however, lacks physical meaning since the equation of motion is described in terms of the unknown fictitious loads $\mathbf{b}_1$ and $\mathbf{b}_2$. For this reason an alternative formulation is suggested and the equation of motion is re-written in terms of the unknown tangential $\mathbf{u}$ and normal $\mathbf{w}$ displacement components. Therefore, using eqs (43) and (44) the unknown fictitious loads $\mathbf{b}_1$ and $\mathbf{b}_2$ can be written as

$$\mathbf{b}_1 = \mathbf{T}_1^{-1}\mathbf{u}, \quad \mathbf{b}_2 = \mathbf{T}_2^{-1}\mathbf{w} \tag{56), (57}$$

After their substitution in eqn (55), we obtain the equation of motion in terms of the displacement components

$$\mathbf{M}\begin{bmatrix} \ddot{\mathbf{u}} \\ \ddot{\mathbf{w}} \end{bmatrix} + \mathbf{C}\begin{bmatrix} \dot{\mathbf{u}} \\ \dot{\mathbf{w}} \end{bmatrix} + \mathbf{K}\begin{bmatrix} \mathbf{u} \\ \mathbf{w} \end{bmatrix} = \begin{bmatrix} \mathbf{p}_t \\ \mathbf{p}_n \end{bmatrix} \tag{58}$$

with

$$\mathbf{M} = \begin{bmatrix} \mathbf{M}_1 & \mathbf{0} \\ \mathbf{0} & \mathbf{M}_2 \end{bmatrix}, \quad \mathbf{C} = \begin{bmatrix} \mathbf{C}_1 & \mathbf{0} \\ \mathbf{0} & \mathbf{C}_2 \end{bmatrix}, \quad \mathbf{K} = \begin{bmatrix} \mathbf{K}_{11} & \mathbf{K}_{12} \\ \mathbf{K}_{21} & \mathbf{K}_{22} \end{bmatrix} \tag{59), (60), (61}$$

being the mass matrix, damping matrix, and stiffness matrix, respectively.

Eqn (58) can be solved numerically, using any time step integration technique, to establish the time dependent vectors $\mathbf{u}$ and $\mathbf{w}$. Substituting these vectors in eqs (56) and (57) to evaluate the fictitious loads $\mathbf{b}_1$ and $\mathbf{b}_2$, and consequently apply the latter in eqs (45) - (50), we finally obtain the displacements derivatives at the N nodal points in the interior of the beam.

4 NUMERICAL EXAMPLES

4.1 Vibrations of symmetric tapered circular arches

In order to validate our proposed model, as a first example, we study the vibrations of clamped circular arches with symmetric tapered rectangular cross-section of constant width $b = 20\text{mm}$ and linearly varying height $h(s) = h_0\left(1-2\eta s/l\right)$ for $0 \le s \le l/2$ and $h(s) = h_0\left(1+2\eta s/l\right)$ for $l/2 \le s \le l$, where h_0 is the height of the cross-section at the crown, η is the taper ratio, $l = R\theta$ the length of the arch with θ being the arch opening angle (see Fig. 2). The data employed are: $E = 6.89\times10^{10}\,\text{N/mm}^2$, $\rho = 2770\text{kg/m}^3$, $R = 750\text{mm}$ and $h_0 = 4\text{mm}$. In Table 1 numerical results for the non-dimensional fundamental natural frequency $\bar{\omega} = \omega R^2\sqrt{\rho A_0/EI_0}$ is presented for various values of the arch opening angle. In the same table, results derived previously by Tufekci and Yigit [14], Öztürk et al. [15] and Karami and Malekzadeh [16] are also presented. By comparison, the results of the proposed method agree very well with the existing ones.

Taper ratio η	Angle θ (deg)	This study	Tufekci & Yigit [14]	Öztürk et al. [15]	Karami and Malekzadeh [16]
0.0	20	504.11	-	-	-
	30	223.11	-	-	-
	40	124.97	-	-	-
	50	79.78	-	-	-
0.1	20	536.02	538.95	535.42	535.45
	30	237.24	238.07	236.50	236.52
	40	132.86	132.78	131.90	131.91
	50	84.76	84.06	83.50	83.51
0.2	20	567.39	568.30	566.67	566.82
	30	251.13	251.09	250.36	250.34
	40	140.62	140.08	139.67	139.71
	50	89.67	88.72	88.45	88.48
0.3	20	598.04	597.30	597.42	597.72
	30	264.82	263.95	264.00	264.14
	40	148.28	147.29	147.32	147.40
	50	94.51	93.32	93.32	39.38

Table 1 : Non-dimensional fundamental natural frequency of symmetric tapered circular arches for various values of the arch opening angle in example 4.1

4.2 Seismic response of circular arches

The second example examines the seismic response of non-uniform circular arches with a varying rectangular cross-section. Three cases of height variation are considered, namely: (i) uniform cross-section with height $h = 0.75m$, (ii) cross-section of linearly varying height $h(s) = h_0\left(1-2\eta s/l\right)$ for $0 \le s \le l/2$ and $h(s) = h_0\left(1+2\eta s/l\right)$ for $l/2 \le s \le l$ with $h_0 = 0.5\text{m}$ and $\eta = 1$, and (iii) section of parabolically varying section with $h(s) = 6h_0\left(s/l\right)^2 - 6h_0\left(s/l\right) + 2.5h_0$ and $h_0 = 0.5\text{m}$. The properties of the three arches are: $E = 33\times10^6\,\text{kN/m}^2$, $\rho = 2.5\text{ton/m}^3$, $R = 65\text{m}$, $\theta = 45.23973^\circ$, $L = 50\text{m}$, $H = 5\text{m}$ and $b = 1\text{m}$. In order to allow a fair comparison among the three examples, their geometry is adjusted so that they have the same material volume, equal to 38.49m^3.

The natural frequencies and eigenperiods of the first five modes are shown in Table 2. The three arches are subsequently subjected to two strong ground motion records. The acceleration time histories of the ground motions are shown in Fig. 3. The plot of Fig. 3a refers to the Imperial Valley (15 Oct 1997) earthquake, while the second ground motion is the Loma Prieta (18 Oct 1989) record.

In all our analyses, both records are scaled so that their peak ground acceleration is equal to 0.5g. Fig. 4, shows the vertical displacement response histories at the apex (also known as the “crown”) of the three arches for the two ground motions considered. The peak displacement values are marked with a blue circle at the time instant that the vertical displacement at the apex received its maximum value. The corresponding displacement profiles are given in Fig. 5. Horizontal displacement histories are not shown since, in general, they receive

smaller values than the vertical ones. The response histories in Fig. 4, show that the arch of the parabolic section is stiffer and hence exhibits smaller displacements, while the first arch, of the uniform cross-section, is the most flexible. Fig. 5 shows the displacement profiles of the three arches (multiplied by 500). It is observed that the maximum vertical and horizontal displacements (denoted with different marks) receive their maximum values at the quarters of the arch length. The shape of the profile is practically the same for all three arches and both ground motions, while it is also symmetric with respect to a vertical axis passing from the apex (note that no gravity loads are present here).

Fig. 6 shows the base shear response histories, which provide the sum of the horizontal forces at every time instant. The response histories are the same for the three arches as they have the same total mass. The two ground motions once scaled to the same peak ground acceleration have very close spectral accelerations and therefore for both records the maximum base shear is very close and slightly below 500kN. Furthermore, Fig. 7 shows the distribution of the peak horizontal (lateral) inertia forces of the left half of each arch. Inertia forces are calculated as the product of mass times acceleration. It is evident that maximum inertia forces are developed approximately at the mid-height, and tend to slightly reduce towards the apex. Inertia forces are considerably larger for the arch of the uniform cross-section, which was already shown to exhibit larger displacements. Finally, Fig. 8 shows also the distribution of the peak vertical inertia forces which appear approximately at the first and the third quarter of its length. At the apex, the peak vertical forces are always equal to zero, while again inertia forces applied on the first arch are significantly larger than those applied on the third.

	Arch 1 - case (i)	Arch 2 - case (ii)	Arch 3 - case (iii)
ω_1 (T_1)	18.14 (0.346)	19.35 (0.325)	20.35 (0.309)
ω_2 (T_2)	31.20 (0.201)	36.28 (0.173)	33.63 (0.187)
ω_3 (T_3)	53.36 (0.118)	52.90 (0.119)	54.45 (0.115)
ω_4 (T_4)	59.42 (0.106)	59.59 (0.105)	59.57 (0.105)
ω_5 (T_5)	90.63 (0.069)	92.07 (0.068)	88.72 (0.071)

Table 2 : Natural frequencies and eigenperiods of the three circular arches

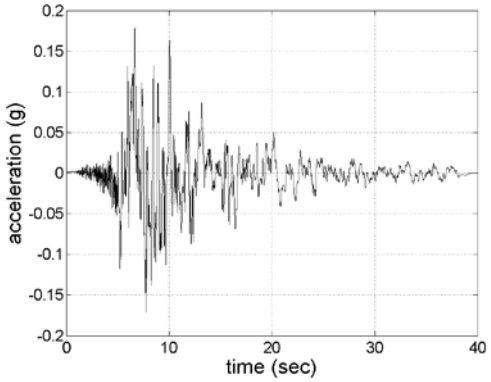

(a) Imperial Valley record

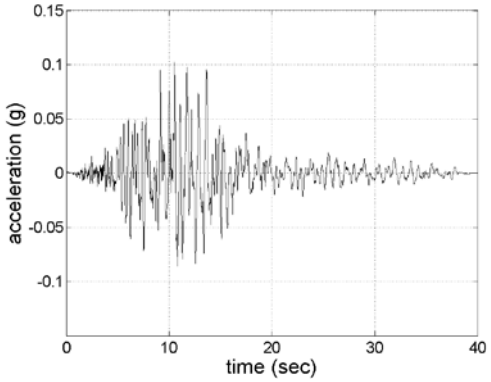

(b) Loma Prieta record

Figure 3. The ground motion time histories adopted (unscaled).

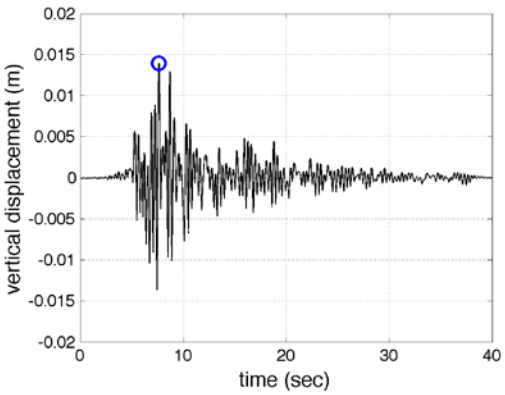

Arch 1 - case (i)

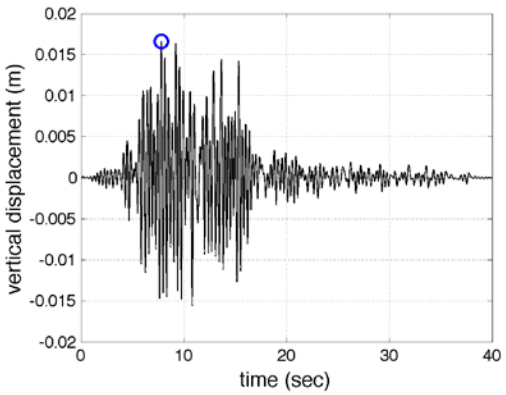

Arch 1 - case (i)

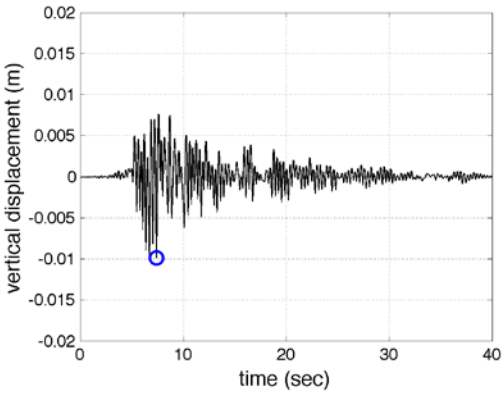

Arch 2 - case (ii)

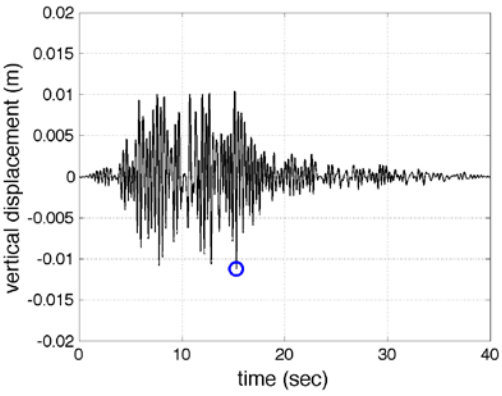

Arch 2 - case (ii)

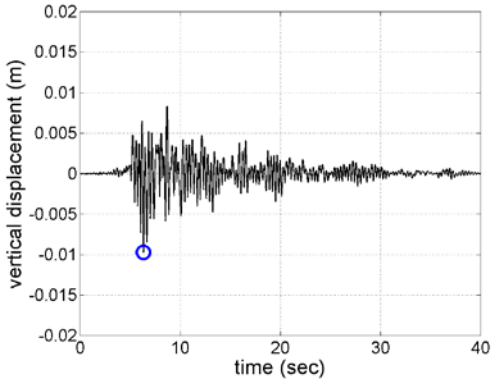

Arch 3 - case (iii)

(a)

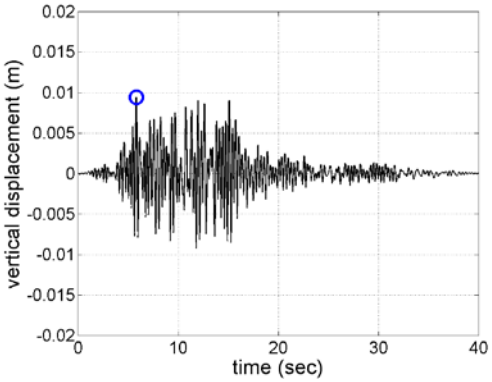

Arch 3 - case (iii)

(b)

Figure 4. Response histories of maximum vertical displacement: (a) Imperial Valley record (left column), (b) Loma Prieta record (right column).

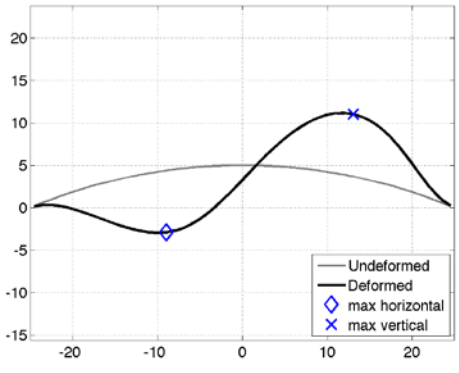

Arch 1 - case (i)

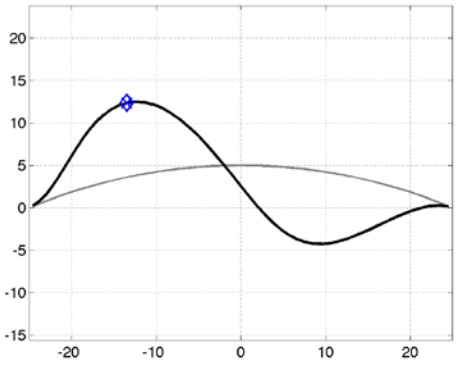

Arch 1 - case (i)

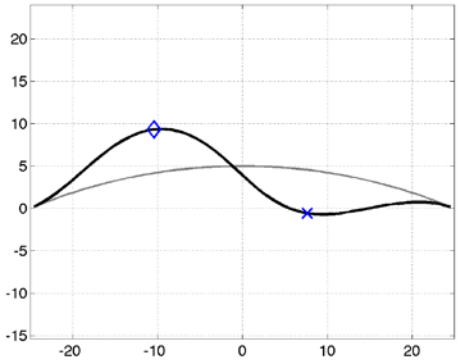

Arch 2 - case (ii)

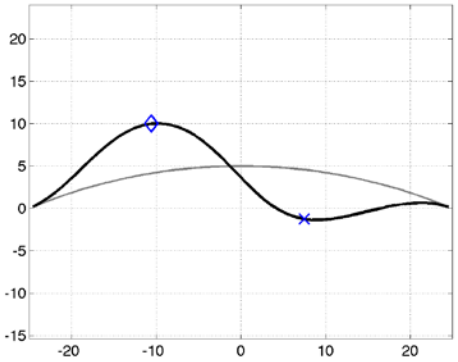

Arch 2 - case (ii)

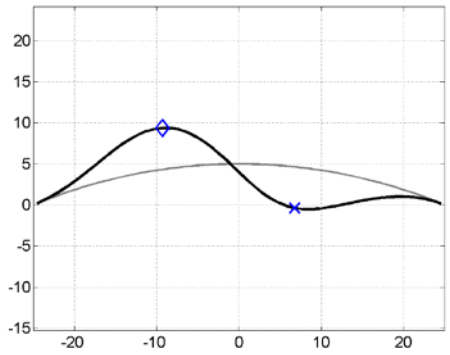

Arch 3 - case (iii)

(a)

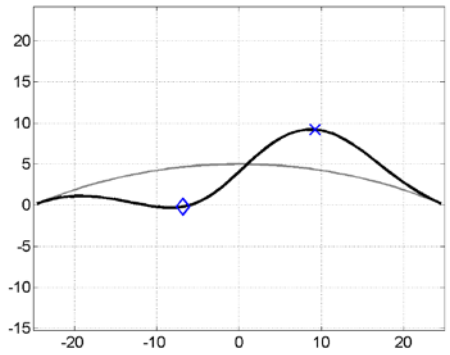

Arch 1 - case (iii)

(b)

Figure 5. Displacement profiles (multiplied by 500): (a) Imperial Valley record (left column), (b) Loma Prieta record (right column).

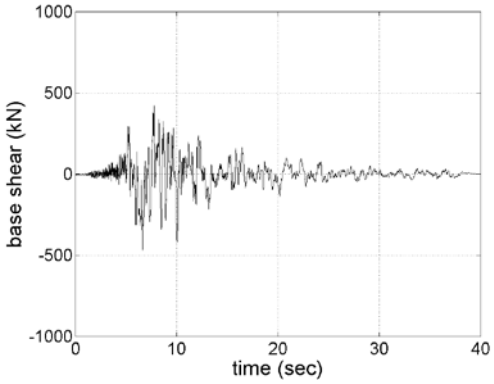

(a)

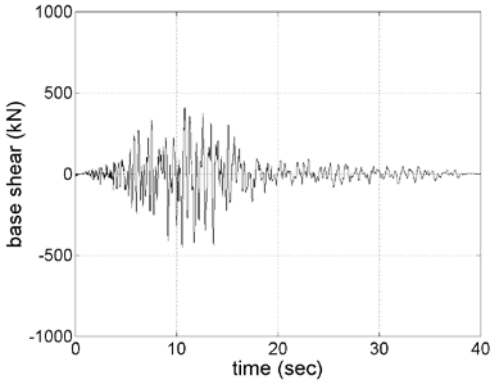

(b)

Figure 6. Base shear response history: (a) Imperial Valley record (left column), (b) Loma Prieta record (right column).

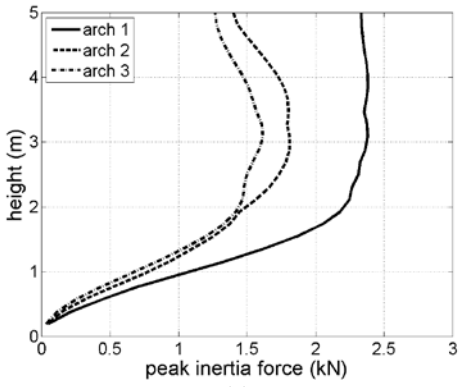

(a)

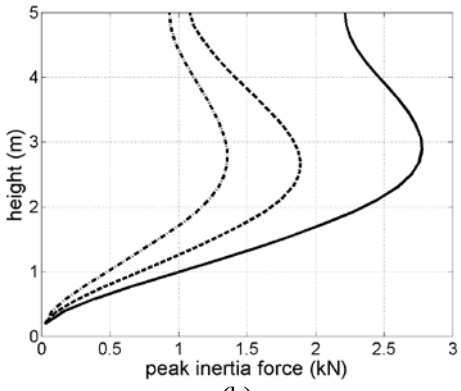

(b)

Figure 7. Profiles of peak horizontal inertia forces: (a) Imperial Valley record, (b) Loma Prieta record.

5 CONCLUSIONS

The paper presents a novel method for the seismic assessment of arch structures. A new approach for calculating the stiffness and the mass matrix has been discussed. The proposed approach follows the Analog Equation Method and can handle a variety of problems with respect to the cross-section properties of the arch. Two examples are provided, clearly demonstrating the features of the proposed seismic analysis approach for arched structures. From the presented results, it is concluded that the arch of the parabolic section is stiffer and hence exhibits smaller displacements, while the first arch, of the uniform cross-section, is the most flexible. Moreover, the inertia forces applied on the first arch (both horizontal and vertical) are significantly larger than those applied on the third.

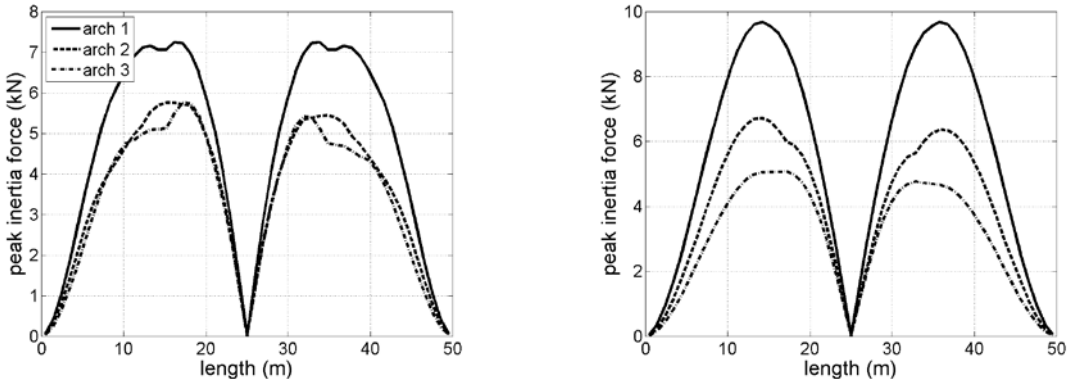

(a) (b)

Figure 7. Profiles of peak vertical inertia forces: (a) Imperial Valley record, (b) Loma Prieta record.

6 REFERENCES

[1] Laura, P.A. and Verniere de Irassar, P.L. (1988), "A note on in-plane vibrations of arch-type structures of non-uniform cross-section: the case of linearly varying thickness", *Journal of Sound and Vibration*, Vol. 124, pp. 1–12.

[2] Gutierrez, R.H., Laura, P.A., Rossi, R.E., Bertero, R. and Villaggi, A. (1989), "In-plane vibrations of non-circular arcs of non-uniform cross-section", *Journal of Sound and Vibration*, Vol. 129, pp. 181–200.

[3] Tong, X., Mrad, N. and Tabarrok, B. (1998), "In-plane vibration of circular arches with variable cross-sections", *Journal of Sound and Vibration*, Vol. 212, pp. 121–140.

[4] Shin, Y.J., Kwon, K.M. and Yun, J.H. (2008), "Vibration analysis of a circular arch with variable cross-section using differential transformation and generalized differential quadrature", *Journal of Sound and Vibration*, Vol. 309, pp. 9–19.

[5] Chidamparam, P. and Leissa, A.W. (1995), "Influence of centerline extensibility on the in-plane free vibrations of loaded circular arches", *Journal of Sound and Vibration*, Vol. 183, pp. 779-795.

[6] Dusseau, R.A. and Wen, R.K. (1989), "Seismic responses of deck-type arch bridges", *Earthquake Engineering and Structural Dynamics*, Vol. 18, pp. 701-715.

[7] Hao, H. (1993), "Arch responses to correlated multiple excitations", *Earthquake Engineering and Structural Dynamics*, Vol. 22, pp. 389–404.

[8] Hao, H. (1995), "Ground motion spatial variation effects on circular arch responses", *Journal of Engineering Mechanics, ASCE*, Vol. 120, pp. 2326–2341.

[9] Usami, T., Lu, Z.H., Ge, H.B. and Kono, T. (2004), "Seismic performance evaluation of steel arch bridges against major earthquakes. Part 1: Dynamic analyses approach", *Earthquake Engineering and Structural Dynamics*, Vol. 33, pp. 1355–1372.

[10] Usami, T., Lu, Z.H., Ge, H.B. and Kono, T. (2004), "Seismic performance evaluation of steel arch bridges against major earthquakes. Part 2: Simplified verification procedure", *Earthquake Engineering and Structural Dynamics*, Vol. 33, pp. 1337–1354.

[11] Slivker, V. (2007), *Mechanics of Structural Elements, Theory and Applications*, Springer-Verlag Berlin Heidelberg.

[12] Katsikadelis, J.T. and Tsiatas, G.C. (2004), "Nonlinear dynamic analysis of beams with variable stiffness", *Journal of Sound and Vibration*, Vol. 270, pp. 847-863.

[13] Katsikadelis, J.T. and Tsiatas, G.C. (2006), "Regulating the vibratory motion of beams by shape optimization", *Journal of Sound and Vibration*, Vol. 292, pp. 390-401.

[14] Tufekci, E. and Yigit, O.O. (2013), "In-plane vibration of circular arches with varying cross-sections", *International Journal of Structural Stability and Dynamics*, Vol. 13, No. 1, 1350003.

[15] Ozturk, H., Yesilyurt, I. and Sabuncu, M., (2006) "In-plane stability analysis of non-uniform cross sectioned curved beams", *Journal of Sound and Vibration*, Vol. 296, pp. 277-291.

[16] Karami, G. and Malekzadeh, P. (2004) "In-plane free vibration analysis of circular arches with varying cross-sections using differential quadrature method", *Journal of Sound and Vibration*, Vol. 274, pp. 777-799.